Instantaneous rest-frame transformation method for temporally induced pair creation

Q. Z. Lv,[1] A. Vikartofsky,[2] S. Norris,[2] Y. J. Li,[1] R. Wagner,[2] Q. Su,[2,3] and R. Grobe[2]
[1]*State Key Laboratory for GeoMechanics and Deep Underground Engineering China University of Mining and Technology, Beijing 100083, China*
[2]*Intense Laser Physics Theory Unit and Department of Physics, Illinois State University, Normal, Illinois 61790-4560, USA*
[3]*Beijing National Laboratory for Condensed Matter Physics, Institute of Physics, Chinese Academy of Sciences, Beijing 100190, China*
(Received 1 January 2014; published 14 April 2014)

We introduce a computational method to determine the rate of the electron-positron pair creation triggered by a time-dependent subcritical external field. It is based on constructing a Lorentz transformation to an instantaneous rest frame, for which the pair-creation rate can be determined by standard techniques. We will discuss the accuracy and efficiency of this method by comparing its predictions with exact time-dependent quantum field theoretical solutions to the Dirac and Klein-Gordon equations for various space-time dependent external fields.

DOI: 10.1103/PhysRevA.89.042105 PACS number(s): 12.20.−m, 03.30.+p, 23.20.Ra, 03.70.+k

I. INTRODUCTION

One of the most intriguing predictions of quantum electrodynamics is the creation of electron-positron pairs from the vacuum due to an extremely strong electric field [1]. Experimental attempts to verify this prediction have been made beginning in the 1980s with heavy ion collisions [2,3], but the observed positrons were likely due to the unavoidable nuclear processes and not triggered by the combined supercritical Coulomb field of both ions. However, in the coming years [4] it might become possible to break down the vacuum by using laser fields with extremely high intensity, which would provide a first and unambiguous evidence of this important quantum field theoretical prediction [5].

There are mainly two intrinsically different mechanisms to create electron-positron pairs from the vacuum. The first one dating historically back to Sauter [6] and Schwinger [7] is based on a time-independent external field that is supercritical, i.e., the associated electric potential times the electronic charge exceeds twice the electron's rest mass energy. Formally it is related to the energy degeneracy between states that (without any interaction) are associated with the positive and negative energy continuum. While many theoretical works focus on predictions for suitable laboratory conditions [8–14], others, including our own, are devoted to the fundamental study of the general principles underlying particle pair creation [15–18].

In addition to the Schwinger mechanism, it is predicted that particles can also be created even for a subcritical field, if the field has a suitable temporal dependence instead. Here the creation process can be associated with induced transitions between states of both energy continua. However, the corresponding calculations are much too challenging for general fields that vary in time in addition to their spatial dependence. As a result of this difficulty, a complete understanding of the precise condition for the temporal dependence to create particles is generally lacking but rather desired in view of the planned laboratory experiments that are naturally based on time-dependent fields.

So far both mechanisms were studied separately and the linkage between these pair-creation criteria is presently not understood. In this work we have chosen a simple model system to bring these two mechanisms together, by proposing an approximate computational method that tries to establish a connection between the pair-creation thresholds for time-dependent subcritical and time-independent supercritical potentials.

The purpose of this work is threefold: First we examine the simplest case of a subcritical electric potential barrier moving at constant velocity and show that the usual supercriticality condition for static fields ($q\Delta V > 2mc^2$) leads to a sharp threshold law for a "supercritical" speed. This is based on the fact that two observers in the lab frame and the field's rest frame detect the same number of created particles. Here the predictions in the field's rest frame can be obtained exactly by a suitable Lorentz transformation. Second, we will generalize this approach to compute the pair-creation rates for more general but still simple time-dependent systems. Finally, we generalize the pair-creation criterion to the case of a moving potential well to gain a deeper understanding of the time-dependent effects in the more general setting.

This paper is organized as follows: In Sec. II we discuss the Dirac and Klein-Gordon equations and the numerical solution of quantum field theories for fermions and bosons in an external potential. In Sec. III we describe the basic idea behind the instantaneous rest-frame transformation (IRFT) method. In Sec. IV we test this method by investigating the pair production rates for various time-dependent potential barriers and also moving potential wells. Finally, in Sec. V we conclude with a discussion and an outlook.

II. THE MODEL SYSTEMS AND THE COMPUTATIONAL METHOD

A. Pair creation from the Dirac and Klein-Gordon equations

If we neglect the mutual interaction between electrons and positrons, the creation of the particle-antiparticle pairs by an external field $V(x,t)$ can be described by the Dirac equation [19] (in atomic units where $m = \hbar = 1$ a.u., $q = -1$, and $c = 137.036$ a.u.), with the one-dimensional Hamiltonian,

$$h = c\sigma_1 p_x + c^2\sigma_3 + qV(x,t). \tag{2.1a}$$

Here σ_i are the usual 2×2 Pauli matrices. In order to keep the problem numerically tractable, we have reduced

the dynamics to one dimension assuming spatial uniformity in the other two dimensions. This reduction allows us to describe the states by two-component wave functions $\phi(x,t) = [\phi_1(x,t),\phi_2(x,t)]^T$ instead of the usual ones based on four components.

Similarly, the creation of boson-antiboson pairs can be modeled in the Feshbach-Villars representation [20] by the Klein-Gordon Hamiltonian,

$$h_B = (\sigma_3 + i\sigma_2)p_x^2/2 + c^2\sigma_3 + qV(x,t). \tag{2.1b}$$

As the quantum field theoretical approach to determine the pair-creation rate numerically for any external potential is rather standard by now, we briefly review it in Appendix A. The space-time dependent external fields that we study below are based on a Sauter potential barrier $V(x) \equiv V_0 S(x)$ with the smooth unit-step function $S(x) \equiv [1 + \tanh(x/w)]/2$. Here w denotes the spatial turn-on width, which is identical to the spatial extension of the associated electric field pulse, $E(x) = -dV(x)/dx$. In Sec. IV we also study a moving potential well, modeled by $V(x) = V_0[S(x + \frac{D}{2}) - S(x - \frac{D}{2})]$, where the distance D is the total extension of the well.

B. The pair-creation rate for the time-independent potentials

As our proposed method is based on relating the space-time dependent potentials $V(x,t)$ to a time-independent one, we review here first a solution technique for constant force fields. For this special case, there are numerous techniques available to calculate the pair-creation rate. For example, according to Hund's rule [21] the pair-creation rate in the long-time limit can be expressed as

$$\Gamma = 1/(2\pi)\int T(E)dE, \tag{2.2}$$

where $T(E)$ is the transmission coefficient as a function of energy and the integral is over the range of energies, $c^2 \leqslant E \leqslant -c^2 + V_0$, where Klein tunneling [22–26] occurs when $V_0 > 2c^2$. For the special case of the smooth barrier $V(x) \equiv V_0 S(x)$ the transmission coefficients can be computed analytically for the Dirac equation (2.1a) as well as the Klein-Gordon equation (2.1b). They take the form

$$T_F(E) = \frac{\sinh[\pi p(E)w]\sinh[\pi q(E)w]}{\sinh\{\pi[V_0/c + p(E) - q(E)]w/2\}\sinh\{\pi[V_0/c - p(E) + q(E)]w/2\}}, \tag{2.3a}$$

$$T_B(E) = \frac{\cosh\{\pi[p(E) - q(E)]w\} - \cosh\{\pi[p(E) + q(E)]w\}}{\cosh[\pi\sqrt{(wV_0/c)^2 - 1}] + \cosh\{\pi[p(E) - q(E)]w\}}, \tag{2.3b}$$

for fermions (T_F) and bosons (T_B), respectively [27]. Here $p(E)$ and $q(E)$ are the momenta of the particles at a point where $V(x) = 0$ and $V(x) = V_0$ and are equal to $p(E) = \sqrt{(E^2/c^2) - c^2}$ and $q(E) = \sqrt{[(E - V_0)^2/c^2] - c^2}$. Systematic tests of predictions of these two expressions were made in Ref. [27].

III. THE PROPOSED INSTANTANEOUS REST-FRAME METHOD

The general interaction of either fermions or bosons with an external force of arbitrary spatial and temporal dependence is modeled here by the scalar potential $V(x,t)$. At a particular instant in time, denoted by t_i, we can define an instantaneous velocity v_i via the ratio of the temporal and spatial derivative of the potential, $v_i \equiv -[\partial V(x,t_i)/\partial t_i]/[\partial V(x,t_i)/\partial x]$. For example, when applied to the special case of a shape-invariant moving potential, $V(x,t) = U[x - X(t)]$, this definition would predict a position-independent velocity, $v_i = \partial X/\partial t_i$, as expected.

We then perform *formally* a Lorentz transformation of the system into a new frame with coordinates $(x',\ t')$ that is moving with this velocity v_i along the positive x direction relative to the original lab frame. Thus the γ parameter for the Lorentz transformation between the two frames is given by $\gamma \equiv [1 - (v_i/c)^2]^{-1/2}$ at that time. In general, a Lorentz transformation rule characterized by an arbitrary γ would lead to a nonvanishing vector potential $A'_x(x',t')$ along the x direction. However, due to the special relationship of γ with v_i in the original potential, the curl and the temporal derivative of $A'_x(x',t')$ vanish identically, such that it only affects the definition of the canonical momentum and therefore can be neglected. Equivalently, there is no magnetic field in one spatial direction. The Lorentz transformed scalar potential is given by $V'(x',t') = \gamma V(x,t)$ where $x \equiv \gamma(x' + vt')$ and $t \equiv \gamma(t' + vx'/c^2)$. We refer to this potential V' as the (instantaneous rest-frame transformed) IRFT potential from now on.

For the simplest case of a uniformly moving potential $V(x,t) = U(x - vt)$, we would obtain the IRFT potential $V'(x',t') = \gamma U(x'/\gamma)$ that is exactly at rest and therefore independent of time t'. This is consistent with the fact that an electric field is invariant under a Lorentz transformation along the field direction, i.e., $E'(x',t') = -\partial V'(x',t')/\partial x' = -\gamma\partial U(x'/\gamma)/\partial x' = -\partial V(x,t)/\partial x = E(x)$.

In order to interpret our data in the next sections it is rather important to note that the formal Lorentz transformation rule, $V'(x',t') = \gamma V(x,t)$, would predict the potential seen by a true observer (that moves with the potential $U[x - X(t)]$) only for the very special case where $\partial X/\partial t$ does not depend on time. Once the potential (and correspondingly the observer) accelerates, the above formalism does *not* predict correctly what an actual (accelerated) observer would measure in her frame. However, as we argue below, this loss of a possible interpretation does not necessarily hinder the application of this transformation formalism as a computational technique to approximate the pair-creation rate for a general space-time dependent potential. We will establish its accuracy for several time dependencies in the sections below.

To have concrete working models, we choose in these examples below a potential that evolves as $V(x,t) = V_0/2(1+\tanh\{[x-X(t)]/w\})$ in the lab frame. This particular form leads to the instantaneous Lorentz transformed potential $V'(x') \equiv \gamma V_0/2\{1+\tanh[x'/(\gamma w)]\}$, where $\gamma \equiv [1-(v_i/c)^2]^{-1/2}$ with $v_i = \partial X/\partial t_i$. In other words, we can use the transformed amplitude (γV_0) and width (γw) in Eqs. (2.3a) and (2.3b) to determine the transmission coefficients and Hund's rule to obtain the pair-creation rate in this "instantaneous" frame as $\Gamma' = dN(t_i')/dt_i'$.

Although the lab frame observer who sees a moving potential V and an observer who is at rest with respect to it must agree on how many particles are created, $N(t_i) = N'(t_i')$, they would not agree on the magnitude of the pair production rate, $dN'(t_i')/dt_i' \neq dN(t_i)/dt_i$. The pair production rate is the number of particles per unit time, which the two observers experience differently. Thus, if the Lorentz transformation leads to a potential for which the pair-creation rate can be determined as $dN'(t_i')/dt_i' = \Gamma'$ as calculated by Hund's rule (2.2), then the original observer in the lab frame observes a pair-creation rate $\Gamma = (dt_i'/dt_i)\Gamma' = \Gamma'/\gamma$ as we have to compensate for the time dilation effect.

This leads also to different threshold laws for supercriticality for both observers. The general threshold condition for the onset of the pair creation for a potential *at rest* reads $V_0 > 2c^2$. For the moving observer our moving potential appears at rest and of strength γV_0. As a result, the correct threshold for pair production of a moving potential is $\gamma V_0 > 2c^2$. If an observer moving with the potential is able to detect pairs, all other inertial observers must also observe the pair production. It is worth noting here that this fact is nontrivial, and in fact *noninertial* observers will not, in general, agree about the number of particles in a state, since noninertial observers will observe Rindler quanta [28].

IV. EXAMPLES OF VARIOUS TIME-DEPENDENT FORCE FIELDS

In order to study the IRFT method we will examine below several space-time dependencies. We begin in Sec. IV A with a uniformly moving barrier $X(t) = vt$, which is more than just a consistency check and a test of the expected accuracy. This will also introduce the concept of a critical velocity for pair creation and predict in the limit of large velocities drastic differences between the fermionic and bosonic pair-creation rates. We will then show in Sec. IV B that the IRFT method works well for adiabatically changing velocities but fails to predict the observed oscillatory pair-creation rates for too large accelerations. In Secs. IV C and IV D we will study oscillatory potentials for which the velocity is reversed abruptly and finally one where the velocity changes continuously. In order to model the binding potential of a moving nucleus, we combine the two barriers to form a moving binding well in Sec. IV E.

A. Constantly moving force field, $X(t) = vt$

We will begin our numerical analysis of the accuracy of the proposed method for the simplest case of a potential that moves shape invariant with a constant velocity v, $V(x,t) = U(x-vt)$. In this case the instantaneous rest-frame transformation method is supposed to be exact. The usual condition for the permanent pair creation in a supercritical potential at rest $[V_0 > 2c^2]$ leads directly to a corresponding *critical threshold velocity* for the onset of temporally induced pair creation triggered by a moving potential. The corresponding (instantaneous rest-frame) IRFT potential $V'(x')$ has an effective amplitude of $V_0' = \gamma V_0$. In other words, in this frame this condition for supercriticality $(V_0' > 2c^2)$ translates to $\gamma V_0 > 2c^2$. This means that the very motion of an otherwise subcritical potential (with $V_0 < 2c^2$) can produce pairs, if the velocity v just exceeds the sharp threshold value,

$$v_{\rm crit} = \left[1 - V_0^2/(4c^4)\right]^{1/2} c. \tag{4.1}$$

We will show below, that while according to Eq. (4.1) these critical velocities are obviously identical for the Dirac and Klein-Gordon equations, the corresponding pair-creation rates in the limit of $v \to \infty$ are rather different for fermions and bosons. As we have argued in the Introduction, the temporally induced pair creation is usually associated with transitions between states of the positive and negative energy continuum. We presently do not understand how this *sharp* velocity threshold could be predicted from a picture that is based on transitions based on photons. Apparently there must be a complete shutoff of any couplings (including all multiphoton processes) between these states as soon as we have $v < v_{\rm crit}$.

To give a specific numerical example, we choose the subcritical potential height $V_0 = 1.9c^2$ with a width of $w = 0.5/c$ in all cases below. If this force field does not change in time, we would not observe any particles. According to Eq. (4.1) the threshold velocity for this V_0 is $v_{\rm crit} = 0.31c$. In Fig. 1 we monitor the time dependence of the number of created fermions and bosons $N(t)$ for three potentials that evolve with three speeds $v = 0.4c$, $0.5c$, and $0.6c$.

We see that after a short time period the number of particles for both systems grows linearly in time with characteristic rates that depend on the magnitude of the potential's velocity. As expected the rate increases with the velocity of the potential barrier.

In Fig. 2 we have graphed by the dots the numerically determined slopes of $N(t)$ for the long-time limit for the fermionic and bosonic simulations as a function of the potential's velocity v. The slope was obtained from the numerical data $N(t)$ by the least-squares fitting method of a straight line using the closest ten temporal grid points at each side of the time t. It is clear that particles can only be created if the velocity exceeds $v > 0.31c$, in full agreement with Eq. (4.1). The two curves are based on the IRFT method using Hund's formula of Eq. (2.2).

The agreement is excellent. However, this is expected as the IRFT method should be exact in the special case where the potential moves with a constant velocity.

While the bosonic and fermionic pair-creation rates seem to follow a similar pattern, they have a rather different behavior if the potential's speed v approaches c. In fact, for a velocity close to c the two graphs even cross. This is related to the formally different expressions for the transmission coefficient in Eq. (2.3). In the limit of $v \to \infty$

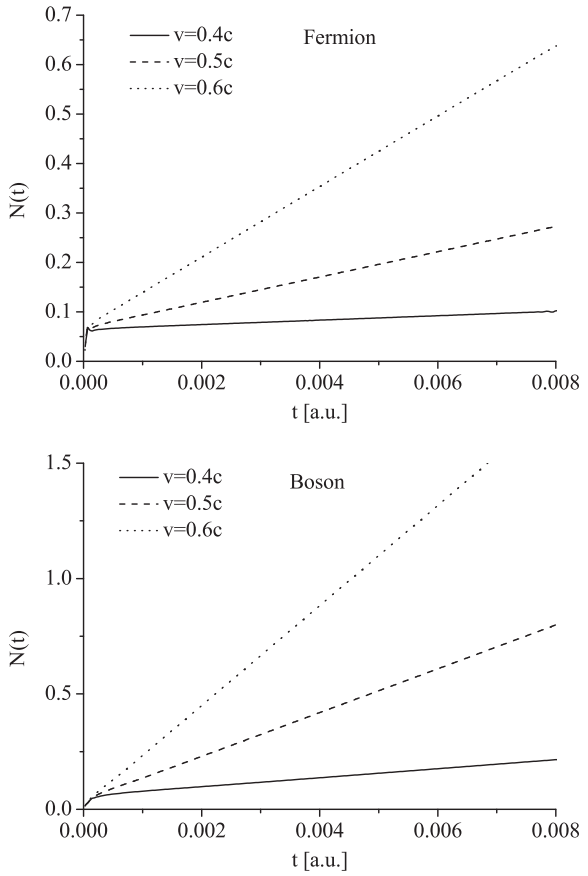

FIG. 1. The number of particle pairs $N(t)$ as a function of time t that were created by a moving potential barrier $V(x,t) = U(x - vt)$ moving with three velocities v. The top (bottom) is for fermions (bosons). $V_0 = 1.9c^2$, $w = 0.5/c$, the numerical box of length $L = 1.0$ a.u. was discretized into $N_x = 1024$ grid points, and the time was sampled at $N_t = 8000$ grid points.

(corresponding to $\gamma \to \infty$) we have $\gamma V_0 \to \infty$. In this limit the fermion transmission coefficient (and therefore the fermion pair-creation rate) tends to infinity while the bosonic coefficient approaches a finite value. As $\gamma \to \infty$, $w \to \infty$, $|q(E) - p(E)|$ is nearly the same as $|q(E) + p(E)|$ in this limit, the numerator in Eq. (2.3b) approaches zero, and as a result the boson creation rate approaches a constant value close to 566.7.

B. Force field moving with an adiabatically changing velocity, $X(t) = v(t)t$

While the perfect agreement between the IRFT method and the exact rates was expected for a potential that moves with a constant velocity, the validity of this approach is not at all clear if the potential accelerates. We have therefore studied a force field $V(x,t) = U[x - v(t)t]$ where the instantaneous velocity $v(t)$ was increased very slowly from $v = 0$ to $v(t) = 0.8c \sin^2[t\pi/(2T_v)]$.

In Fig. 3 we show the corresponding rate computed as the derivative of the numerical data for $N(t)$ for a slowly and more rapidly increasing velocity, corresponding to the time $T_v = 0.0048$ a.u. In order to avoid any pairs that were solely triggered

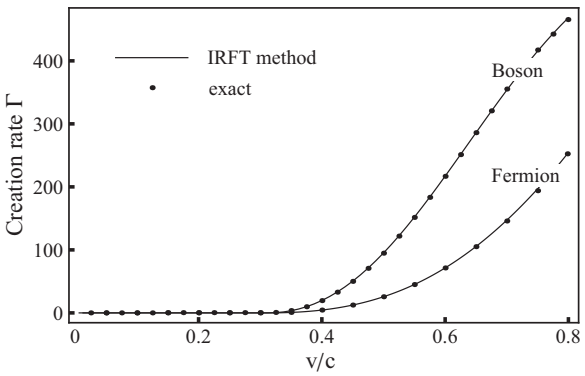

FIG. 2. The pair-creation rate Γ as a function of velocity of the potential barrier $V(x,t) = U(x - vt)$. When the barrier's speed exceeds the critical velocity $(0.312\,25c)$, the creation rate increases with velocity. The exact rates are obtained from the slopes of the numerically obtained $N(t)$, while the IRFT method is based on Hund's rule. $V_0 = 1.9c^2$, $w = 0.5/c$, the numerical box of length $L = 1.0$ a.u. was discretized into $N_x = 1024$ grid points, and the time was sampled at $N_t = 8000$ grid points.

due to a too abrupt turn on, the overall amplitude of the potential was turned on slowly from $V_0 = 0$ to $V_0 = 1.9c^2$ during the early time interval from -0.0005 a.u. $< t < 0$ a.u., while the velocity was ramped up from $v = 0$ only after time $t = 0$ a.u.

We have also included in the figure the prediction due to the IRFT method. The differences are due to two competing mechanisms: A nonzero acceleration always leads to higher-frequency components that would naturally increase the pair-creation rate Γ. As the IRFT method is solely based on the instantaneous velocity, it cannot account for this mechanism and we would expect $\Gamma_{\mathrm{IRFT}} < \Gamma$ in this regime. The early time regime seems to be dominated by this mechanism. For longer times a second (rate-suppressing) mechanism sets in. It is based on the fact that the accelerating force field is able to catch up with the particles that were created before. These particles can inhibit the pair-creation process. As the IRFT method assumes

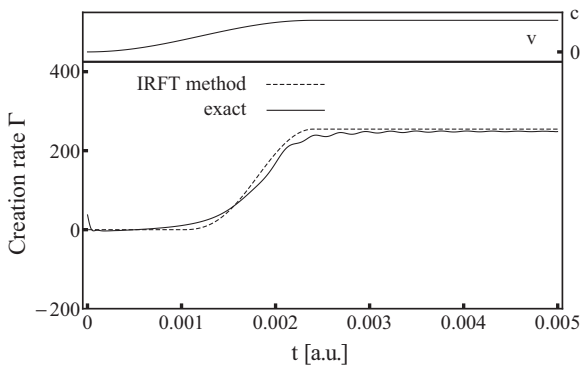

FIG. 3. The creation rate Γ of electron-positron pairs as a function of time t that were created by a moving potential barrier $V(x,t) = U(x - vt)$ whose velocity v increased slowly from $v = 0$ to $v = 0.8c$ during a time interval of duration T_v, as shown by the top curve. For comparison, the prediction due to the IRFT method is shown by the dashed line. $T_v = 0.0024$ a.u., $V_0 = 1.9c^2$, $w = 0.5/c$, the numerical box of length $L = 2.0$ a.u. was discretized into $N_x = 1024$ grid points, and the time was sampled at $N_t = 16\,000$ grid points.

that the front edge of the potential does not encounter these particles, it naturally predicts a higher rate, $\Gamma < \Gamma_{\mathrm{IRFT}}$. The data in the figures suggest that this is the dominant mechanism for longer times. Overall, it is clear that in the adiabatic case the method works fine, while for a rapidly changing velocity the exact rate has an oscillatory behavior that cannot be predicted from the approximate IRFT method. The latter predicts always a monotonic dependence between the instantaneous velocity and the pair-creation rate Γ. It is interesting to note, however, that the temporally asymptotic rate after the oscillations have damped out agrees very well again with the IRFT prediction.

C. Force field with sudden velocity reversals, $X(t) = \pm vt$

We will now study the applicability of our method for a potential that moves with constant speed, but reverses periodically its direction of motion instantly after time intervals of length T each. We stress here again that due to the (infinite) accelerations at specific times $t_n = nT(n = 1,2,3,\dots)$ the Lorentz transformation based formalism does not correctly describe the pair-creation rate that a true (periodically accelerated) noninertial observer (moving with the potential) would detect.

In Fig. 4 we show the pair-creation rate as a function of time for a simple case where the velocity changed instantaneously from $v = 0.8c$ to $v = -0.8c$. After the initial turn-on dependent behavior, the instantaneous rate $\Gamma(t)$ settles to a constant value Γ_∞, corresponding to approximately 254 particles per unit time. This value agrees roughly with the one predicted by the IRFT method for $v = 0.8c$, as indicated by the constant dashed line.

At the moment the velocity reverses, the rate is momentarily reduced even below zero, suggesting that the created pairs are annihilated again. After a small delay of roughly 5×10^{-5} a.u. the acceleration dip is then followed by a drastic spike, suggesting a strongly enhanced rate. The rate oscillates and damps out from below to a constant value, approximately Γ_∞. As this transient behavior cannot be predicted by the IRFT method, it is important to understand the mechanisms responsible for this transient behavior. We should note that it is not possible to predict the acceleration burst by the IRTF method, as the Lorentz based technique only describes inertial observers. In order to analyze the acceleration bursts we are therefore confined to the lab frame, in which the barrier moves to the right during the first half cycle. In order to test the conjecture if the suppression is related to the Pauli blocking for fermions, we have repeated the same simulation for bosons and found that the pattern here is exactly opposite. Here the velocity reversal is accompanied first by a spike in the rate, and the IRFT rate is then approached from above.

In order to better estimate the time it takes for the true creation rate Γ to approach the one predicted by the IRFT method, we have shown in Fig. 5 the corresponding spatial densities of the electron as well as positrons. We have outlined in Appendix B how the corresponding densities $\rho(e^-; x,t)$ and $\rho(e^+; x,t)$ can be computed. We just mention here that for consistency, the area under these densities corresponds to the total number of created particle pairs, $\int \rho(e^-; x,t)dx = \int \rho(e^+; x,t)dx = N(t)$.

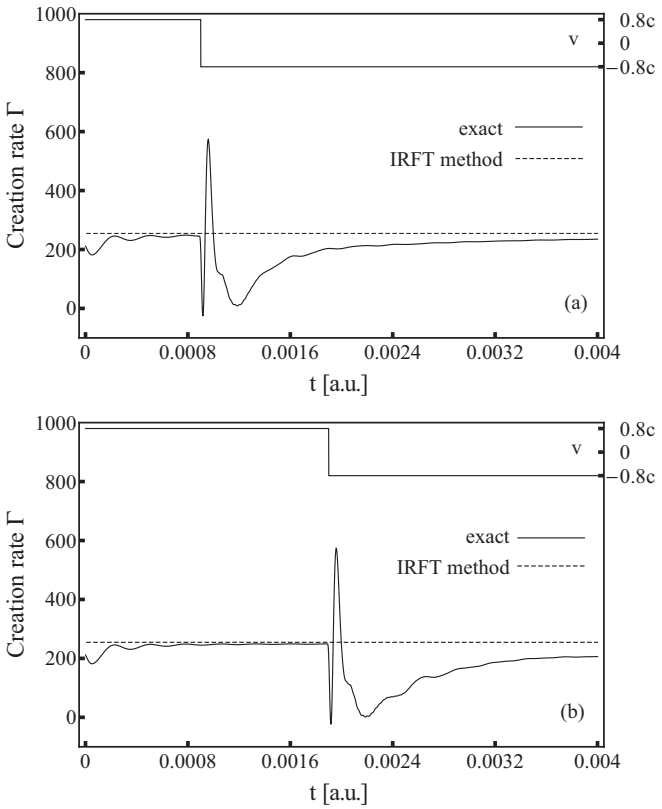

FIG. 4. The creation rate Γ of electron-positron pairs as a function of time t that were created by a moving potential barrier $V(x,t) = U(x - vt)$ whose velocity v was reversed at time T_v, as shown by the top curve. For comparison, the prediction due to the IRFT method is shown by the dashed line. (a) reversal at time $T_v = 0.0009$ a.u.; (b) reversal at time $T_v = 0.0019$ a.u. $V_0 = 1.9c^2$, $w = 0.5/c$, the numerical box of length $L = 2.0$ a.u. was discretized into $N_x = 1024$ grid points, and the time was sampled at $N_t = 16\,000$ grid points.

There are four distinct time regimes. The density in Fig. 5(a) taken at time $t = 2.0 \times 10^{-4}$ a.u. (before the velocity reversal) shows that the electronic and positronic densities have entirely different shapes. This can be understood from the point of view of a rest-frame observer that evolves with the potential to the right with velocity $v = 0.8c$. In this frame the two types of particles are ejected equally to both sides of the potential, the electrons to the left and the positrons to the right. The associated velocity distribution is a complicated convolution of the velocity density at the moment of the particles' creation with the distribution due to the (almost classical) after-acceleration in the force field [30]. If we assume for simplicity that the majority of the particles are created with vanishing speeds in the spatial region where the force is maximum [corresponding to the potential $V'(x' = 0) = \gamma V_0/2$], the energy conservation for a particle inside and outside the force region, $c^2 + \gamma V_0/2 = (c^4 + c^2 p'^2)^{1/2}$ would predict the gained outgoing momentum $p' = \pm\{\gamma V_0 + [\gamma V_0/(2c)]^2\}^{1/2}$. For our specific parameters ($v = 0.8c$ and $V_0 = 1.9c^2$) these particular momenta correspond to $p' = \pm 2.38c$ and correspondingly the particles' velocities $v'_p = c^2 p'/[c^4 + c^2 p'^2]^{1/2} = \pm 0.922c$. If we now transform these two velocities back to the original frame (in which the potential

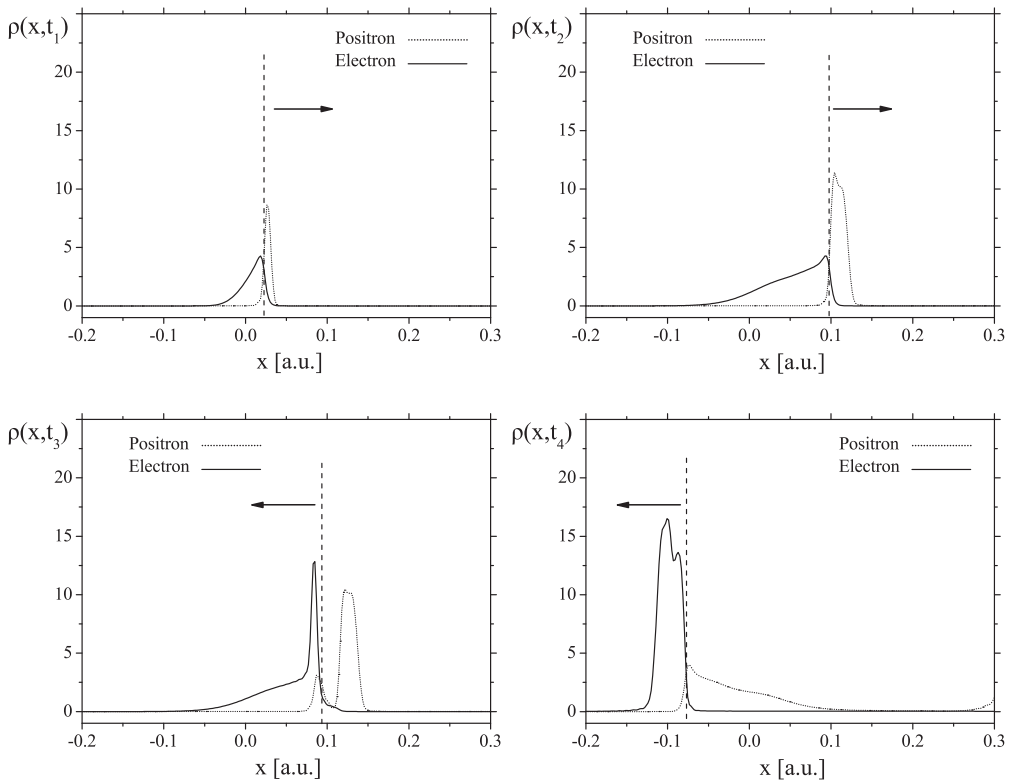

FIG. 5. Temporal snapshots of spatial density of the electrons (solid) and positrons (dotted line) at four moments in time. The vertical dashed line is the location of the force field. (a) $t = 2.0 \times 10^{-4}$ a.u.; (b) $t = 8.9 \times 10^{-4}$ a.u., the time when the velocity of the potential $0.8c$ was reversed; (c) $t = 1.02 \times 10^{-3}$ a.u., after the reversal; (d) $t = 2.51 \times 10^{-3}$ a.u., after the force field has caught up with the priorly created electrons. $V_0 = 1.9c^2$, $w = 0.5/c$, the numerical box of length $L = 2.0$ a.u. was discretized into $N_x = 1024$ grid points, and the time was sampled at $N_t = 16\,000$ grid points.

moves with a speed of $v = 0.8c$) via the usual velocity addition rule, we find $v_p(e^{\pm}) = (\pm v'_p - v)/(1 + v'_p v/c^2)$, leading to $v_p(e^-) = -0.07c$ and $v_p(e^+) = 0.99c$. In other words, the (right-going) positrons move with nearly the speed of light, while the electrons are left behind almost at rest.

This drastic difference with respect to the emission velocities has also significant consequences for the corresponding spatial densities. While the densities $\rho'(e^{\pm}; x',t')$ are (except for a mirror symmetry around $x' = 0$) identical, the Lorentz transformed densities $\rho(e^{\pm}; x,t)$ (as seen in the lab frame) are drastically different. We note that the area under both densities is identical and also agrees with the corresponding area observed in the rest frame of the potential, $\int \rho(e^{\pm}; x,t)dx = \int \rho'(e^{\pm}; x',t')dx'$.

Figures 5(a) and 5(b) show that the electronic density $\rho(e^-; x,t)$ that is left behind develops a quasitriangular shape with a height $\max[\rho(e^-; x,t)] = \rho_{\max}(e^-)$ that does not depend on time and whose location agrees with the position of the maximum of the moving force. This constant value reflects the steady-state ejection rate (particle number flux) from the potential region. The length of the basis of the triangular density increases in time and matches roughly the distance the (maximum of the) force field has passed, $L = 0.8ct + 0.07ct$. It is clear that therefore the area of this triangle increases linearly in time as expected for the total number of particles.

While the electronic density is left behind to the left of the potential, the created positrons are ejected faster than the moving potential. As a result the corresponding density is much higher as it is concentrated only in the smaller spatial domain between the potential at $x = 0.8ct$ and the light front $x = ct$. In other words, the positronic density is about four and a half times narrower than the electronic density, reflecting the ratio of the extensions of the permitted spatial domains, $(0.8ct–0.07ct)/(0.99ct–0.8ct)$.

Figures 5(c) and 5(d) show the densities after the force has reversed its velocity. The force "plows" through the formerly created triangular electronic density. This corresponds precisely to the temporal region in Fig. 4 where the rate of particle creation Γ is much below the rate Γ_{IRFT} as predicted by the IRFT method. The reason for this suppression is obvious. The priorly created electrons could suppress the pair-creation process due to Pauli blocking [26]. This is rather interesting (and possibly even unexpected) as the existing electrons occupy states with rather low momentum, while the left-moving potential would generate new electrons with a very large momentum ($p = -2.38c$) as we have shown above. On the other hand, the left-moving potential leaves now rather slowly moving positrons behind (on the right side of the potential) that could annihilate directly with the (much earlier created) electrons. This second mechanism would suggest that the overall observed decrease of the rate is associated with an annihilation of the newly created slow positions with existing slow electrons rather than a direct reduction of the pair-creation rate. But certainly a much more detailed analysis

would be required to settle these interesting fundamental questions.

The last snapshot [Fig. 5(d)] is taken close to a time when the front edge of the left-going force field has caught up with all slowly moving electrons. If we denote with t_r the time the potential has moved in one direction and t_c the duration of the additional time interval needed for the reversed force to catch up, we can equate the two positions, $-0.07c\ (t_r + t_c) = 0.8c\ (t_r - t_c)$, and obtain $t_c = 1.2t_r$. At this moment $t = 2.2t_r$ the suppression process comes to a halt and the rate is identical to the value of the IRFT method, which is instantaneous and always assumes that there are no priorly created particles in the path of the moving force field. This mechanism gives us now an estimate for the characteristic time scale after which the IRFT method is accurate again. So the longer the time interval the potential has to move in one direction, the longer it takes for the IRFT method to be accurate again after the velocity reversal. This scaling is fully consistent with the scales displayed in Fig. 4.

In order to determine which parameters affect these transient sequences of acceleration caused bursts, we have varied the velocity v of the potential below.

In Fig. 6 we show the rates for two velocity reversals for the barrier. When the velocity changes between $0.64c$ and $-0.64c$, the sudden spike in creation rate is higher as expected. After this spike the creation rate settles down to a value (97.92), which is within 1.95% of that given by the IRFT method. When the velocity changes between $0.4c$ and $-0.4c$, after the spike in the creation this rate also settles back down to a value (4.49) also close to that predicted. When the velocity changes between $0.08c$ and $-0.08c$, it is always significantly less than the critical value of $0.312\,25c$ and the IRFT method fails completely to predict the acceleration burst in the rate.

In Fig. 7 we have kept the speed constant at $\pm 0.5c$, but varied the spatial length of the barrier w where particles can be created. As we kept the total potential height V_0 unchanged,

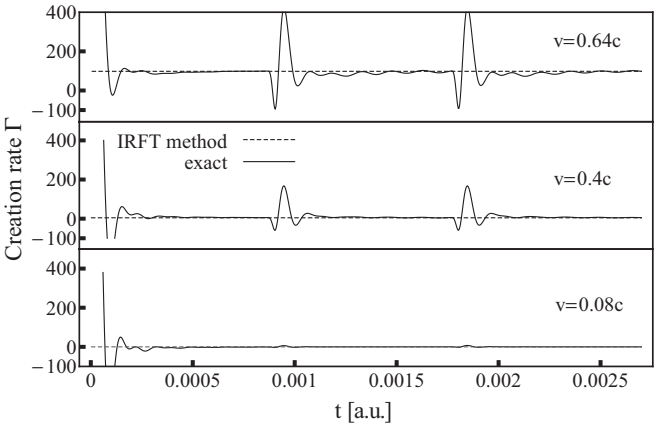

FIG. 6. The creation rate Γ of particle pairs as a function of time t that were created by a moving potential barrier $V(x,t) = U(x - vt)$ whose velocity alternates instantly at times $T = 0.0009n$ between $\pm 0.08c$ (bottom), $\pm 0.4c$ (middle), and $\pm 0.64c$ (top). For comparison, the prediction due to the IRFT method is shown by the dashed line. $V_0 = 1.9c^2$, $w = 0.5/c$, the numerical box of length $L = 1.0$ a.u. was discretized into $N_x = 1024$ grid points, and the time was sampled at $N_t = 8000$ grid points.

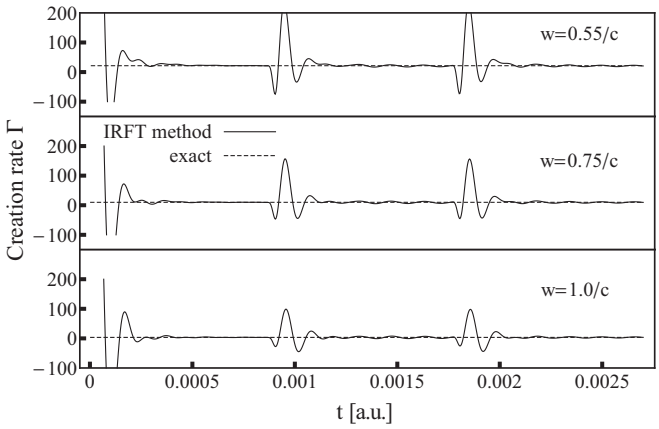

FIG. 7. The creation rate Γ of particle pairs as a function of time t that were created by a moving potential barrier $V(x,t) = U(x - vt)$ whose velocity alternates instantly at times $T = 0.0009n$ between $0.5c$ and $-0.5c$. The widths of the potentials are $w = 0.55/c$ (top), $0.75/c$ (middle), and $1/c$ (bottom). For comparison, the prediction due to the IRFT method is shown by the dashed line. $V_0 = 1.9c^2$, the numerical box of length $L = 1.0$ a.u. was discretized into $N_x = 1024$ grid points, and the time was sampled at $N_t = 8000$ grid points.

an increase of the width w leads to a decreased electric field, which then would decrease the pair-creation rate. The graphs suggest that the change in the width of the electric potential has no major effect on the delay of the creation rate spike, nor on the overall shape of the graph, but narrower potentials do create more particles.

D. Periodically oscillating force field, $V(x,t) = U[x + v(t)t]$

In the above cases, the velocity of the potential was instantly reversed. We will now examine the validity of the IRFT method for a force field that oscillates continuously back and forth, $v(t) = v\sin\omega t$. In the simulation displayed in Fig. 8, where the

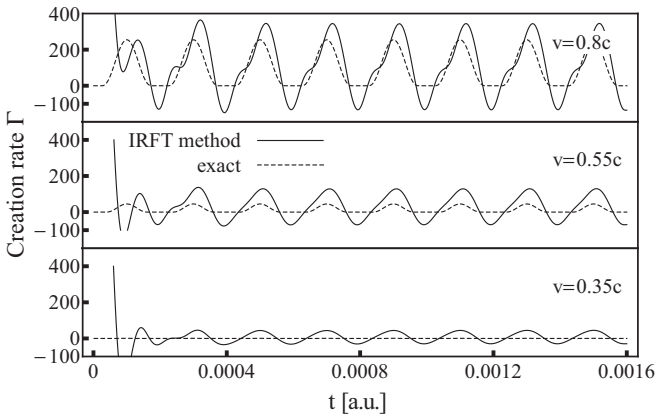

FIG. 8. The creation rate Γ of particle pairs as a function of time t that were created by a potential barrier $V(x,t) = U(x - vt)$ whose velocity oscillates periodically with frequency $\omega = 0.836c^2$ between $\pm 0.35c$ (bottom), $\pm 0.55c$ (middle), and $\pm 0.8c$ (top). For comparison, the prediction due to the IRFT method is shown by the dashed line. $V_0 = 1.9c^2$, $w = 0.5/c$, the numerical box of length $L = 1.0$ a.u. was discretized into $N_x = 1024$ grid points, and the time was sampled at $N_t = 8000$ grid points.

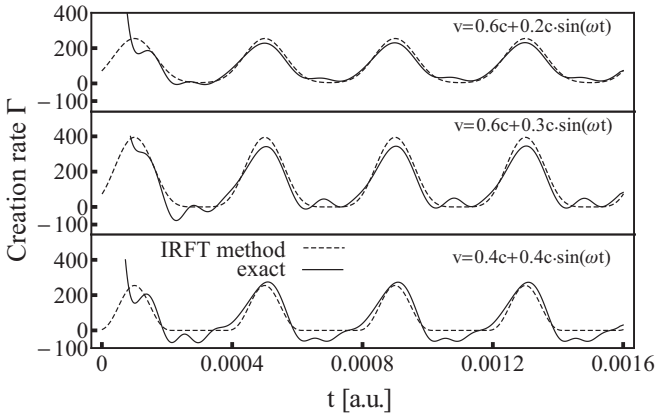

FIG. 9. The creation rate Γ of particle pairs as a function of time t that were created by a potential barrier $V(x,t) = U(x - vt)$ whose velocity oscillates periodically with frequency $\omega = 0.836c^2$ with a constant background velocity. For comparison, the prediction due to the IRFT method is shown by the dashed line. $V_0 = 1.9c^2$, $w = 0.5/c$, the numerical box of length $L = 1.0$ a.u. was discretized into $N_x = 1024$ grid points, and the time was sampled at $N_t = 8000$ grid points.

barrier's velocity oscillates as a sine function, it is clear that the creation rate has no sudden spike but instead increases and decreases smoothly. In addition, the amplitude of the creation rate graph increases as the amplitude of the velocity function increases.

Unlike the graph of a creation rate for a potential that has a constant velocity, the creation rate does not seem to approach the value given by Fig. 2 or predicted by the IRFT method. The pair-creation rate appears to oscillate with a frequency which is twice the frequency of the velocity function, which makes sense as positive and negative velocities lead to the same creation rate.

We conjecture that the mismatch between the exact rate and the one predicted by the IRFT method is due to the unavoidable existence of priorly created particles that come in and out of the interaction zone. We have demonstrated in the spatial density graphs of Fig. 5 that this "catch-up" mechanism leads to a smaller rate than predicted by the IRFT method.

In order to distinguish between the competing effects due to the acceleration and the importance of the catch-up phenomenon (described previously), we have performed a similar simulation as in Fig. 8, but this time the oscillatory motion is superimposed by a constant velocity, $v(t) = v_1 + v_2 \sin \omega t$ in order to simulate a forward drift. If $v_1 > v_2$ the force field cannot return to those spatial regions in which particles where created in the past. In this way we can minimize the interaction of the front edge of the force field and priorly created particles.

In Fig. 9 we see an overall rather good agreement between the IRFT method and the exact data. The agreement is best for $v_1 = 0.6c$ and $v_2 = 0.2c$ shown by the upper panel. Here the true rate Γ is positive at nearly all times. It is rather interesting to observe that precisely during those time intervals when the velocity decreases from its maximum value the IRFT method overestimates the rate, whereas during most of the positive acceleration phases it underestimates the rate. At those instants of time when the velocity is maximum, the acceleration vanishes and the IRFT method overestimates the maximum rate. The fact that the IRFT method and the exact rate predict the precise times when the rates are maximum also suggests that the pair-creation mechanism responds without any appreciable delay to the changes in the velocity.

The middle panel shows the dynamical response for the two velocities $v_1 = 0.6c$ and $v_2 = 0.3c$, where there are moments in time when the total velocity is below critical as indicated by the time intervals when $\Gamma_{\mathrm{IRFT}} = 0$. While the moments in time at which the rate peaks are still rather accurately predicted by the IRFT method, it overestimates the rates when $v = 0.9c$.

In the situation depicted in the bottom panel ($v_1 = 0.4c$ and $v_2 = 0.4c$) the potential can come to a complete stop. These extended regions are characterized by a negative rate $\Gamma < 0$. As the IRFT method is not able to predict a negative rate Γ_{IRFT} for any velocity, it is not surprising that it is not valid here. But it works still qualitatively well in cases where the true dynamics has a positive rate Γ. We also note that the true maximum rate is not observed to occur at those times when the speed is maximum ($v = 0.8c$).

It is worth mentioning that the adiabatic parameter [29] defined as $\chi = eE/(mc\omega)$ comes out to be roughly 4.5 for the runs presented in Figs. 8 and 9. This means that indeed we are in the adiabatic rather than the multiphoton limit. In this estimate we assumed $E \approx V/w = 1.9c^2/(0.5/c) = 3.8c^3$, which may not be an accurate estimation as the potential determines the dynamics for a localized field and not necessarily the electric field. It is also interesting to note that while the numerical value for χ in Figs. 8 and 9 is the same, the match with the IRFT method is much better for Fig. 9. The introduction of the drift in this figure is thus important in addition to parameter χ.

E. Uniform motion of a binding force field

In the sections above, we focused on a time-dependent barrier and found that even a subcritical potential can trigger the pair creation if it moves with a sufficiently large speed. In this section we will show that the pair creation triggered by a force field that represents a binding potential well is surprisingly rather different than that associated with a moving barrier. We will see that here the threshold behavior for the critical velocity differs for fermions and bosons, in fact there are multiple thresholds, and also their long-time pair creation is different. As we restrict our analysis here on a binding potential that moves with a constant velocity, the IRFT method is exact. The Hund rule, however, is no longer applicable and we could use numerical diagonalization techniques instead.

The pair creation associated with a moving binding potential has been studied in the past in the context of the collisions of two relativistic heavy ions [1]. Here the phenomenological Hamiltonian describes a moving Coulomb potential to model the motion of the two ions. In our numerical study below, we choose a one-dimensional localized well $V(x) = V_0[S(x + \frac{D}{2} - vt) - S(x - \frac{D}{2} - vt)]$, where D is the extension of the potential well and v is its velocity. The function $S(x)$ is again the smooth step function (Sauter potential) as we used in the prior sections. Even though our model is simple, it can give us some insight into how the motion affects the pair production process. To be specific, we have chosen a subcritical peak potential value $V_0 = 1.6c^2$ and

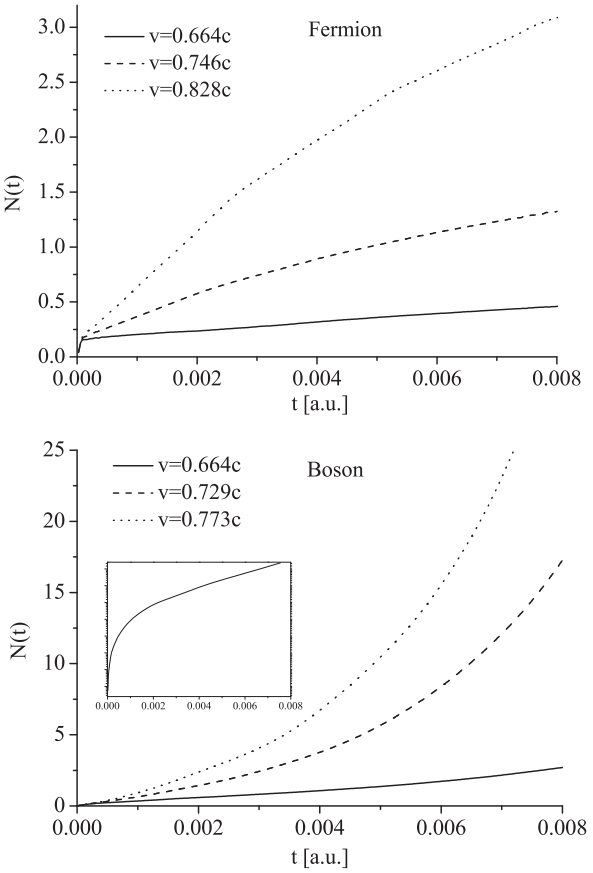

FIG. 10. The number of particle pairs N as a function of time t that were created by a potential well $V(x,t) = U(x - vt)$ moving with three velocities. The top (bottom) is for fermions (bosons). The inset shows the long-time behavior of the boson on a logarithmic scale. $V_0 = 1.6c^2$, $w = 0.3/c$, $D = 6.4/c$, the numerical box of length $L = 1.0$ a.u. was discretized into $N_x = 1024$ grid points, and the time was sampled at $N_t = 8000$ grid points.

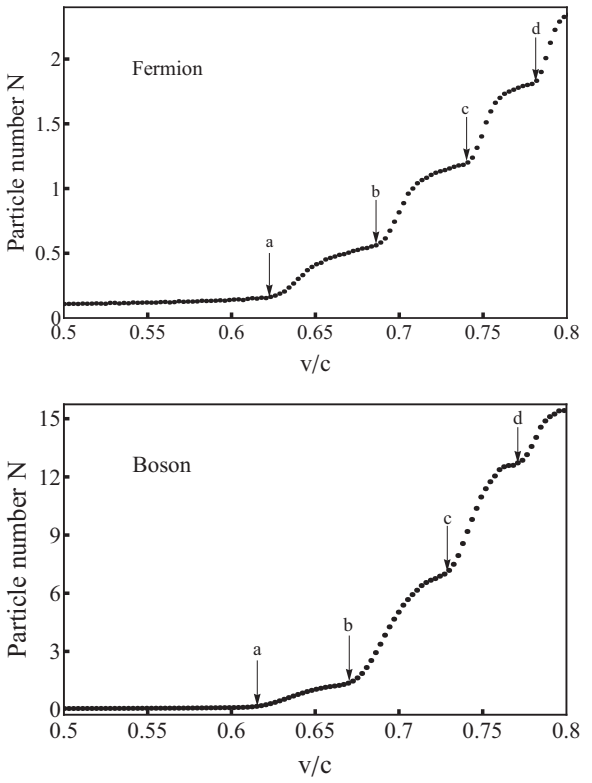

FIG. 11. The final number of particle pairs N as a function of the velocity v of the moving potential well $V(x,t) = U(x - vt)$. The top (bottom) is for fermions (bosons) at final time $t = 0.008$ a.u. ($t = 0.0065$ a.u.). The parameters are the same as in Fig. 10.

a width of each edge equal to $w = 0.3/c$. In this case any pair production is entirely induced by the time dependence of the potential.

To get started, we display in Fig. 10 the time dependence of the number of created particles for three velocities, $v = 0.664c$, $0.746c$, and $0.828c$ for fermions and $v = 0.664c$, $0.729c$, and $0.773c$ for bosons.

The graphs reveal a qualitative difference between the fermionic and bosonic behavior.

While for fermions the signal $N(t)$ rises, its slope reduces and after a very long time it saturates to a constant value; for bosons the particle number increases exponentially [31] after the initial phase. To confirm this long-time exponential feature, we display in the inset of Fig. 10 $N(t)$ for $v = 0.773c$ on a logarithmic scale.

The saturation for fermions and the exponential growth for bosons in Fig. 10 is well expected from previous works on time-independent, but supercritical, potential wells [31,32]. For fermions the Pauli blocking prohibits the continued creation of fermions as the bound states associated with the potential get occupied [33]. For bosons a kind of inverse process is observed. The spontaneous-emission-like process for bosons enhances the pair creation. Here the occupation of bosonic bound states actually induces an even more rapid pair creation. This leads to an exponential-like growth of the pair creation where the exponent is a function of the single barrier creation rate and the edge to edge separation as was discussed in Ref. [31].

In order to find out the factors that affect the long-time creation behavior for different velocities v of the potential well more systematically, we display the particle number at the final time as a function of the velocity v in Fig. 11 for both systems. We see that the particle number is rather small and practically negligible for small velocities but then increases after v exceeds a critical value. This behavior is similar to that shown in Fig. 2 for the moving barrier. However, the critical values for fermions and bosons are different. For our choice of parameters ($V_0 = 1.6c^2$) the critical velocity (for a single barrier) according to Eq. (4.1) would amount to $v_{\rm crit} = 0.6c$. As we will show below for both systems the true onset of pair creation occurs at slightly larger velocities, $v_{\rm crit} = 0.623c$ (for fermions) and $v = 0.616c$ (for bosons). This suggests that the corresponding criteria for a potential barrier and potential well are different and also differ for fermions and bosons.

In addition to the different onset, both graphs also reveal a stepwise growth of $N(t)$, suggesting that there is more than just a single relevant characteristic velocity. We have marked the corresponding discrete velocity values by the arrows in the figure. We note that the pair-creation rate increases very sharply after these velocities.

Due to the (temporally) constant velocity for each simulation, the IRFT method is exact and we can analyze our potential in its own rest frame where it is given by $\gamma V(x'/\gamma)$. To develop the criterion for the onset of supercriticality and to understand the step structure of Fig. 11, we analyze below the spectrum for the corresponding full Hamiltonians based on the static potential $\gamma V(x'/\gamma)$.

In contrast to the barrier where the onset of supercriticality is given by the height of the barrier ($V_0 > 2c^2$) a binding potential can generate pairs if the energy of its lowest-lying bound state is below $-c^2$; i.e., it is embedded into the negative energy continuum. This is referred to as bound state "diving" into the Dirac sea [33].

In Fig. 12 we display the lower-energy spectrum of the Hamiltonian with the potential $\gamma V(x'/\gamma)$ as a function of the velocity. As we increase v the parameter γ increases leading to an increasing binding strength γV_0 as well as a spatial widening of the IRFT potential. As the potential gets deeper and wider, more discrete bound states can dive into the negative energy continuum. For example, in the case of the fermionic system, starting at $v_{\rm crit} = 0.629c$, $0.694c$, and $0.746c$, we have one, two, and three bound states in the continuum, whereas the bosonic system requires the velocities $0.621c$, $0.677c$, and $0.732c$, respectively. We note that while the IRFT potential is identical for each system, the stationary Dirac and Klein-Gordon Hamiltonians of Eqs. (2.1a) and (2.1b) predict different spectra.

The numerical values for the four lowest critical velocities read of the spectra match very well the onset velocities for an increased number of particle pairs as displayed in Fig. 11 by the arrows. It is therefore clear that the step structure of $N(t)$ as a function of the velocity is directly related to the additional bound states that have dived into the negative continuum.

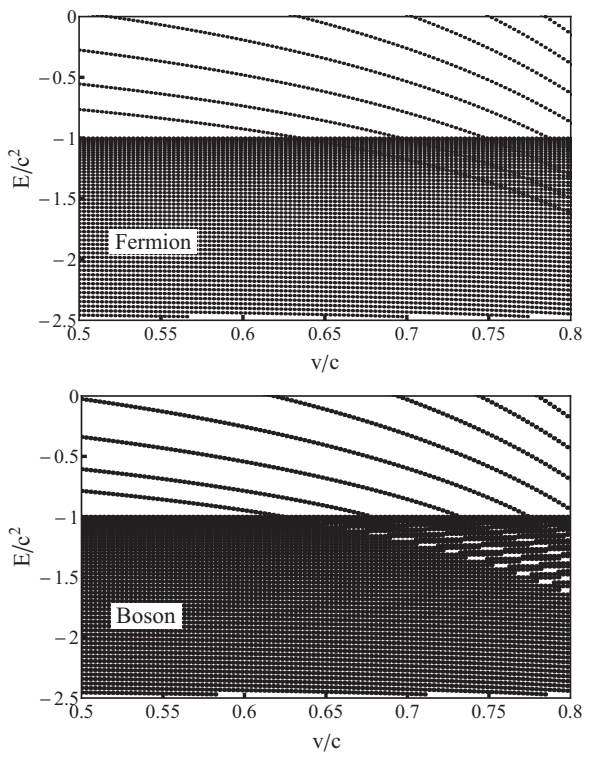

FIG. 12. The energy spectrum as a function of the velocity v for the fermionic (top) and bosonic (bottom) systems. $V_0 = 1.6c^2$, $w = 0.3/c$, $D = 6.4/c$, and the numerical box of length $L = 0.5$ a.u. was discretized into $N_x = 512$ grid points.

V. DISCUSSION AND OUTLOOK

The purpose of this work has been to introduce a computational method to calculate the pair-creation rate caused by arbitrary external force fields and to examine its accuracy. It is based on mapping the time-dependent potential onto an approximate but static one, for which various computational methods (such as Hund's rule or numerical diagonalization) are available. While it is, in principle, approximate in nature it can provide access to estimating the pair creation yield for any three-dimensional electromagnetic configuration. In this paper we have focused on two special cases of potentials. They were assumed to be subcritical at rest and their time evolution was assumed to be shape invariant; i.e., $V(x,t) = U[x - X(t)]$. While these constraints are not severe with respect to describing the fields of moving nuclei, studies for more general space-time dependencies should be performed.

In principle, any general time-dependent (even subcritical) force should be able to trigger the creation of electron and positron pairs due to unavoidable transitions of the negative to the positive energy states. However, the IRFT method when applied to the special case of a uniformly moving potential predicts a sharp threshold velocity below which no pairs are created. It is presently not clear how this threshold could be predicted from an (equivalent) picture that is based on the energy spectrum of the potential, which should be sufficiently broad to contain frequencies that could trigger multiphoton transitions. In future work it would be interesting to explore whether a general condition can be found to determine whether a completely general potential $V(x,t)$ has the capacity to produce particle pairs.

We also point out that it is nontrivial to obtain the most effective instantaneous velocity that is required for the IRFT method. The special case of shape-invariant potentials of the form $U[x - X(t)]$ leads to a unique velocity $v_i = \partial X/\partial t_i$ at this particular instant in time t_i. Similarly, if the total potential was characterized by two different velocities, $U[x - X_1(t)] + U[x - X_2(t)]$, we would formally obtain the average $v_i = [\partial(X_1 + X_2)/\partial t_i]/2$ for the effective instantaneous speed. However, it should be obvious that this collective choice for v_i would not be suitable for the IRFT method, which would significantly underestimate the true pair-creation rate. In an ideal situation, one could try to decompose the potential into individual shape-invariant portions, $V(x,t) = \sum_\alpha U_\alpha[x - X_\alpha(t)]$, and then apply to the IRFT method to each component $U_\alpha[x - X_\alpha(t)]$ separately. But from a mathematical point of view, it is very challenging to construct the corresponding transformation schemes to decompose a general space-time dependent potential $V(x, t)$ into its shape-invariant contributions $U_\alpha[x - X_\alpha(t)]$.

Alternatively, in the more general case for $V(x, t)$ the instantaneous velocity is defined via the ratio of the temporal and spatial derivative of the potential, $v_i(x) \equiv -[\partial V(x,t_i)/\partial t_i]/[\partial V(x,t_i)/\partial x]$, as we argued in Sec. III. This potential is characterized by a position-dependent velocity.

The majority of the particles are usually created in those spatial regions where the corresponding amplitude of the electric field $E(x,t_i) = -\partial V(x,t_i)/\partial x$ is largest, $\max[|E(x,t_i)|] = |E(x_{\max},t_i)|$. We might therefore select $v_i(x_{\max})$ as the effective instantaneous velocity required for the IRFT method, but much more systematic studies to test these conjectures are necessary.

ACKNOWLEDGMENTS

This project was initiated in discussions with Professor S. Hassani. We also enjoyed several helpful discussions with Mr. Y. Liu, Dr. M. Jiang, Dr. Y. T. Li, Dr. X. Lu, Dr. Z. M. Sheng, and Dr. J. Zhang. This work was supported by the NSF, by the National Basic Research (973) Program of China (Grant No. 2013CBA01504), and by the NSFC (Grants No. 11128409 and No. 11374360).

APPENDIX A: NUMERICAL SOLUTIONS OF QED

The quantum field for a particle can be expressed as a sum (or integral) over the force-free plane wave states:

$$\hat{\Psi}(x,t) = \sum_p \hat{b}_p(t) W_p(u;x) + \sum_p \hat{d}_p^\dagger(t) W_{-p}(d;x). \quad \text{(A1)}$$

Here the states $W_p(u;x)$ and $W_p(d;x)$ are the positive and negative energy solutions to the Dirac or Klein-Gordon equation in the absence of any potential, i.e., the plane wave solutions. $\hat{b}_p$ and $\hat{d}_p$ are the annihilation operators for the particle and antiparticle, respectively. Together with the respective creation operators $\hat{b}_p^\dagger$ and $\hat{d}_p^\dagger$ they satisfy the anticommutator relations $\{\hat{b}_p, \hat{b}_{p'}^\dagger\} = \delta_{pp'}$ and $\{\hat{d}_p, \hat{d}_{p'}^\dagger\} = \delta_{pp'}$ for electrons and positrons, and commutator relations $[\hat{b}_p, \hat{b}_{p'}^\dagger] = \delta_{pp'}$ and $[\hat{d}_p, \hat{d}_{p'}^\dagger] = \delta_{pp'}$ for bosons and antibosons, where for our numerical discretized system the delta functions $\delta_{pp'}$ are Kronecker deltas.

The quantum field theoretical Hamiltonian $\hat{H}$ of a particle coupled to an external field is expressible in terms of the first-quantized Dirac Hamiltonian h as $\hat{H} = \int dx \hat{\Psi}(x,t)^\dagger h_F \hat{\Psi}(x,t)$ for fermions and $\hat{H} = \int dx \hat{\Psi}(x,t)^\dagger \sigma_3 h_B \hat{\Psi}(x,t)$ for bosons. It should be noted that, while this Hamiltonian fully accounts for the interaction of the particle to the external field through the minimum coupling principle, which is contained in h, it neglects all internal forces between particles and antiparticles.

The particle annihilation operator $\hat{b}_p(t)$ must satisfy the Heisenberg equation $i\partial\hat{b}_p(t)/\partial t = [\hat{b}_p(t), \hat{H}]$, and similarly for the antiparticle operator $\hat{d}_p(t)$. It follows that the field operator $\hat{\Psi}(x,t)$ must also follow the Heisenberg equation, $i\partial\hat{\Psi}(x,t)/\partial t = [\hat{\Psi}(x,t), \hat{H}]$. Furthermore, since the field operator $\hat{\Psi}(x,t)$ also contains states $W_p(u;x)$ and $W_p(d;x)$, it also satisfies the Schrödinger-like equation $i\partial\hat{\Psi}(x,t)/\partial t = h\hat{\Psi}(x,t)$. The time dependence in the field operator Eq. (A1) may therefore be transferred from the creation and annihilation operators to the states,

$$\hat{\Psi}(x,t) = \sum_p \hat{b}_p W_p(u;x,t) + \sum_p \hat{d}_p^\dagger W_p(d;x,t), \quad \text{(A2)}$$

where we have $\hat{b}_p(t) = \sum_{p'} \hat{b}_{p'} \langle u; p|U(e^-,t)|u; p'\rangle + \sum_{p'} \hat{d}_{p'}^\dagger \langle u; p|U(e^-,t)|d; p'\rangle$ and similarly for $\hat{d}_p^\dagger(t)$. The field operator $\hat{\Psi}(x,t)$ can therefore be constructed from the solutions $W_p(u;x,t)$ and $W_p(d;x,t)$ with $\langle u; p|U(t)|d; p'\rangle$ for fermions and $\langle u; p|\sigma_3 U(t)|d; p'\rangle$ for bosons.

As a side comment, we note that the Hamiltonian for the bosonic system is non-Hermitian, but we can generalize the definition of a Hermitian conjugate for the Klein-Gordon equation. If we redefine the left-hand side eigenvector as $\langle\bar{E}|_g = (\sigma_3|E\rangle)^\dagger$, then the Hamiltonian h_B is generalized Hermitian as $h_B = \bar{h}_B$, where $\bar{h}_B = \sigma_3 h_B^\dagger \sigma_3$.

APPENDIX B: THE TIME EVOLUTION OF THE SPATIAL PROBABILITY DENSITIES $\rho(e^\pm; x,t)$

We note that the total charge density would not allow us to distinguish between the density of the individual electrons and positrons. For example, if an electron and a positron have identical spatial probability densities, then the total charge density could be zero, as if there were no particles at all. It is also therefore not possible to compute the total number of created electron-positron pairs directly from the charge density. In order to be able to distinguish both cases, we have to compute also a spatial probability density for both particles. Consistent with prior works [34], we propose here to define spatial probability densities that are based on the assumption that we can separate the total electron-positron field operator into a positronic and electronic portion,

$$\Psi(t) = \Psi(e^-;t) + C\Psi(e^+;t). \quad \text{(B1)}$$

We would obtain $\Psi(e^-;t) \equiv \Lambda_u \Psi$ and $\Psi(e^+,t) \equiv \Lambda_u C \Psi C$, where Λ_u is the positive energy subspace projector and where C is the charge conjugation operator. This definition allows us also to compute the total number of particles. If we insert the time evolution of the creation and annihilation operators and use their action on the Fock-space operators $Cb_{-p}(t) = b_{-p}^\dagger(t)C$ and $Cd_{-p}^\dagger(t) = d_{-p}(t)C$, we obtain

$$\begin{aligned}\Psi(e^-;t) &= \sum_p b_p(t) W_p(u) \\ &= \sum_p \sum_{p'} [b_{p'} \langle u; p|U(e^-,t)|u; p'\rangle \\ &\quad + d_{-p}^\dagger \langle u; p|U(e^-,t)|d; p'\rangle] W_p(u), \quad \text{(B2a)} \\ \Psi(e^+;t) &= \sum_p d_{-p}(t) W_{-p}(d) \\ &= \sum_p \sum_{p'} [b_{p'}^\dagger \langle d; p|U(e^-,t)|u; p'\rangle^* \\ &\quad + d_{-p'} \langle d; p|U(e^-,t)|d; p'\rangle^*] W_{-p}(d), \quad \text{(B2b)}\end{aligned}$$

where $U(e^-,t)$ is the time evolution operator based on the electronic Hamiltonian (2.1a). In order to construct the probability densities associated with these definitions from an initial field theoretical (second-quantized) state $|\Omega\rangle$ we would compute

$$\rho(e^-;x,t) = \langle\Omega(t=0)|\Psi(e^-;t)^\dagger \Psi(e^-;t)|\Omega(t=0)\rangle, \quad \text{(B3a)}$$

$$\rho(e^+;x,t) = \langle\Omega(t=0)|\Psi(e^+;t)^\dagger \Psi(e^+;t)|\Omega(t=0)\rangle. \quad \text{(B3b)}$$

It is now straightforward to compute the electronic probability density $\rho(e^-;x,t)$ for the vacuum state $|\Omega(t=0)\rangle = |\text{vac}\rangle$ and obtain

$$\rho(e^-;x,t) = \sum_{p'} \left| \sum_{p} \langle u;p|U(e^-,t)|d;p'\rangle W_p(u;x) \right|^2, \quad \text{(B4a)}$$

and similarly for the positronic density $\rho(e^+;x,t)$,

$$\rho(e^+;x,t) = \sum_{p'} \left| \sum_{p} \langle d;p|U(e^-,t)|u;p'\rangle^* W_{-p}(d;x) \right|^2. \quad \text{(B4b)}$$

Here we have used $\langle u;p'|CU(e^-,t)|u;p\rangle = \langle d;-p|U(e^-,t)|u;p\rangle = -\langle u;p|U(e^-,t)|d;-p\rangle^*$.

As a last consistency check we note that the total number of particles, given by $N(t) = \sum_p \langle b_p^\dagger(t) b_p(t)\rangle = \sum_p \langle d_p^\dagger(t) d_p(t)\rangle$ can also be obtained from the integral over both spatial densities,

$$N(t) = \int dx \rho(e^-;x,t) = \int dx \rho(e^+;x,t) = \sum_p \sum_{p'} |\langle u;p'|U(e^-,t)|d;-p\rangle|^2. \quad \text{(B5)}$$

From this quantity, the instantaneous rate of pair production can be defined as $\Gamma(t) = dN(t)/dt$.

According to Eq. (B5), the total number of particle-antiparticle pairs produced as a function of time by a potential $V(x,\ t)$ can be found easily as long as the initial states of the system are given. We have therefore solved the Dirac equation for fermions and Klein-Gordon equation with a split-operator algorithm [35–37] with a numerical box of length L with periodic boundary conditions, and we have used up to $N_x = 2014$ and $N_t = 10\,000$ space- and time-grid points. For our parameters this discretization scheme gave converged results with a numerical error of less than 1%.

[1] W. Greiner, B. Müller, and J. Rafelski, *Quantum Electrodynamics of Strong Fields* (Springer, Berlin, 1985).
[2] T. Cowan, H. Backe, K. Bethge, H. Bokemeyer, H. Folger, J. S. Greenberg, K. Sakaguchi, D. Schwalm, J. Schweppe, K. E. Stiebing, and P. Vincent, Phys. Rev. Lett. **56**, 444 (1986).
[3] I. Ahmad *et al*. (APEX Collaboration), Phys. Rev. Lett. **78**, 618 (1997).
[4] For recent experimental efforts, see, e.g., http://www.eli-beams.eu/
[5] For a recent review, see A. Di Piazza, C. Müller, K. Z. Hatsagortsyan, and C. H. Keitel, Rev. Mod. Phys. **84**, 1177 (2012).
[6] F. Sauter, Z. Phys. **69**, 742 (1931).
[7] J. S. Schwinger, Phys. Rev. **82**, 664 (1951).
[8] R. Alkofer, M. B. Hecht, C. D. Roberts, S. M. Schmidt, and D. V. Vinnik, Phys. Rev. Lett. **87**, 193902 (2001).
[9] C. D. Roberts, S. M. Schmidt, and D. V. Vinnik, Phys. Rev. Lett. **89**, 153901 (2002).
[10] H. Gies and K. Klingmüller, Phys. Rev. D **72**, 065001 (2005).
[11] D. D. Dietrich and G. V. Dunne, J. Phys. A **40**, F825 (2007).
[12] R. Schützhold, H. Gies, and G. Dunne, Phys. Rev. Lett. **101**, 130404 (2008).
[13] G. V. Dunne, Q. H. Wang, H. Gies, and C. Schubert, Phys. Rev. D **73**, 065028 (2006).
[14] F. Fillion-Gourdeau, E. Lorin, and A. D. Bandrauk, Phys. Rev. Lett. **110**, 013002 (2013).
[15] A. I. Nikishov, Nucl. Phys. B **21**, 346 (1970).
[16] A. Hansen and F. Ravndal, Phys. Scr. **23**, 1036 (1981).
[17] B. R. Holstein, Am. J. Phys. **67**, 499 (1999).
[18] M. Jiang, W. Su, Q. Z. Lv, X. Lu, Y. J. Li, R. Grobe, and Q. Su, Phys. Rev. A **85**, 033408 (2012); M. Jiang, Q. Z. Lv, Z. M. Sheng, R. Grobe, and Q. Su, *ibid.* **87**, 042503 (2013).
[19] B. Thaller, *The Dirac Equation* (Springer, Berlin, 1992).
[20] For a review on the properties of the Klein-Gordon Hamiltonian, see, e.g., W. Greiner, *Relativistic Quantum Mechanics*, 3rd ed. (Springer, Berlin, 2000); A. Wachter, *Relativistische Quantenmechanik* (Springer, Berlin, 2005).
[21] F. Hund, Z. Phys. **117**, 1 (1940).
[22] O. Klein, Z. Phys. **53**, 157 (1929); **41**, 407 (1927).
[23] P. J. M. Bongaarts and S. N. M. Ruijsenaars, Ann. Phys. (San Diego) **101**, 289 (1976).
[24] B. R. Holstein, Am. J. Phys. **66**, 507 (1998).
[25] N. Dombey and A. Calogeracos, Phys. Rep. **315**, 41 (1999).
[26] P. Krekora, Q. Su, and R. Grobe, Phys. Rev. Lett. **92**, 040406 (2004).
[27] T. Cheng, M. Ware, Q. Su, and R. Grobe, Phys. Rev. A **80**, 062105 (2009).
[28] N. D. Birrell and P. C. W. Davies, *Quantum Fields in Curved Space* (Cambridge University Press, Cambridge, 1982).
[29] E. Brezin and C. Itzykson, Phys. Rev. D **2**, 1191 (1970); for review, see also V. S. Popov, Phys. Usp. **47**, 855 (2004).
[30] N. Chott, Q. Su, and R. Grobe, Phys. Rev. A **76**, 010101(R) (2007).
[31] R. E. Wagner, M. R. Ware, Q. Su, and R. Grobe, Phys. Rev. A **81**, 052104 (2010).
[32] P. Krekora, K. Cooley, Q. Su, and R. Grobe, Phys. Rev. Lett. **95**, 070403 (2005).
[33] B. Müller, H. Peitz, J. Rafelski, and W. Greiner, Phys. Rev. Lett. **28**, 1235 (1972).
[34] For a review, see Cheng, Q. Su, and R. Grobe, Contemp. Phys. **51**, 315 (2010).
[35] G. R. Mocken and C. H. Keitel, Comput. Phys. Commun. **178**, 868 (2008); M. Ruf, H. Bauke, and C. H. Keitel, J. Comput. Phys. **228**, 9092 (2009).
[36] J. W. Braun, Q. Su, and R. Grobe, Phys. Rev. A **59**, 604 (1999).
[37] A. D. Bandrauk and H. Shen, J. Phys. A **27**, 7147 (1994).